RESEARCH

Exploring the Multifaceted Nature of $TaCu_3X_4(X = S, Se, Te)$ Materials: A DFT Study Revealing Promising Structural, Optoelectronic, Thermodynamic and Thermoelectric Properties

Muhammad Tauqeer[1] · Muhammad Mubashir[1] · Dilbar Khan[2] · Ahmad M. Saeedi[3] · Raed H. Althomali[4] · Gideon F. B. Solre[5] · Muhammad Ehsan Mazhar[6] · Majed M. Alghamdi[7,8] · Adel A. El-Zahhar[7,8] · Sana Ullah Asif[9] · Muhammad Asif Iqbal[10]

Abstract

The present study looks into the $TaCu_3X_4(X = S, Se, Te)$ compounds' structural, mechanical, electronic, thermodynamic, optical, as well as thermoelectric attributes using a First-Principles computational method based on the Density-Functional theory (DFT) methodology. Initially, the implementation of the PBE-GGA approach was done to determine the lattice constants of the understudied compounds. A thorough analysis of the binding energy calculations has been performed to determine the structural stability of selected chemicals. Additionally, the study of elastic stiffness constants is utilized to evaluate the mechanical stability. It has been reported that the $TaCu_3X_4(X = S, Se, Te)$ compounds are mechanically stable due to fulfillment of Born-Stability criteria ($C_{44} < 0$). Through the determination of Pugh's along with passion ratios as well as the Cauchy pressure, the ductile and the brittleness nature of the $TaCu_3X_4(X = S, Se, Te)$ compounds have been established. An analysis of the electronic band structure, total density of states, as well as partial density of states was performed in order to ascertain the electronic features. It has been shown that the compounds $TaCu_3X_4(X = S, Se, Te)$ exhibit indirect band gaps of 1.71, 1.65 and 0.14 eV, respectively. The thermodynamic stability of the materials under investigation was depicted by the computation of the Born-criteria along with binding energy. We have computed and evaluated a number of optical characteristics. In addition to presenting opacity at lower incoming photon energy levels, the selected compounds display considerable optical conductivity as well as absorption coefficients when subjected to energetic beams of photons. Moreover, BoltzTraP coding was utilized to evaluate the examined compounds $TaCu_3X_4(X = S, Se, Te)$ potential for thermoelectric uses. Based on an analysis of the Seebeck coefficient, electric and thermal conductivity, and power factor, it seems that the studied-compounds have potential to be effective candidates for applications in thermoelectric technology.

Keywords Energy and industry · Technology · Electronic materials · DFT calculations · Thermoelectric properties

✉ Muhammad Ehsan Mazhar
dr.ehsan@bzu.edu.pk

✉ Sana Ullah Asif
sanaullahasif@gmail.com

1 Division of Science and Technology, Department of Physics, University of Education, Lahore 54770, Pakistan

2 Centre of Excellence in Solid State Physics, University of the Punjab, Lahore, Pakistan

3 Department of Physics, Faculty of Science, Umm AL-Qura University, 24382 Makkah, Saudi Arabia

4 Department of Chemistry, College of Science and Humanities in Al-Kharj, Prince Sattam Bin Abdulaziz University, 11942 Al-Kharj, Saudi Arabia

5 Department of Chemistry, Thomas J. R. Faulkner College of Science and Technology, University of Liberia, 00231 Monrovia, Montserrado County, Liberia

6 Institute of Physics, Bahauddin Zakariya University, Multan, Pakistan

7 Department of Chemistry, College of Science, King Khalid University, P.O. Box 9004, 61413 Abha, Saudi Arabia

8 Research Center for Advanced Materials Science (RCAMS), King Khalid University, Abha, Saudi Arabia

9 School of Materials and Energy, Yunnan University, Kunming 650091, People's Republic of China

10 University of Management and Technology (UMT), Lahore, Pakistan

1 Introduction

The current growth of the globe has resulted in a significant rise in the need for energy, and the traditional method of producing enormous amounts of energy is causing considerable damage to the ecosystem via the emission of carbon [1–3]. Due to this fact, climate change has become an important concern for humanity, and researchers from every part of the world. In current scenario, material researchers have been concentrating their efforts on the creation of innovative technological innovations that are both sustainable and efficient in terms of energy consumption. As a result of their straightforward crystalline structure, triple inter-metallic AB_3X_4 compounds, which belong to one of the most extensive classes of ternary compounds [4], have been subjected to extensive research. The AB_3X_4 compounds have a number of uses in various sectors, including thermoelectric materials [5] that have substantial uses, such as thermoelectric generators [6], refrigeration systems [7], and numerous other comparable uses. The aforementioned compounds are capable of directly generating electricity through the incorporation of heat. On the other hand, because of the intrinsic complexity of TE materials, their efficiency is very confined.

The class of semiconducting compounds such as Ta-based compounds has attracted significant attention in the last decade, due to its potential in many applications including photovoltaic material and transparent conductor [8]. These facts have contributed to substantial both theoretical as well as practical studies on the aforementioned compounds [9]. The $TaCu_3X_4(X = S, Se, Te)$ compounds have a comparatively low lattice thermal conductivity and are characterized by high degree of anharmonicity [10]. In light of this fact, significant study have described the thermoelectric characteristics of the selected class of materials based on calculations using first principles computational method [4, 9].

In Thonhauser, T., et al. [11] have published the elastic constants of selected class of compounds. Researchers are very interested in exploring the possible useful features of very wide bandgap material because of its structural stability [(VCu_3Se_4 is stable up to 1014 K, NbCu_3Se_4 up to 1206 K and TaCu_3Se_4 up to 1328 K)] [11], earth abundance, and lack of toxicity in its component elements. At a temperature of 1000 K, the S of p-type $TaCu_3Te_4$ may reach 2.36, according to the findings of the researchers of Liu, X.-P., et al. [4], who explored the TE characteristics of $TaCu_3X_4(X = Se, S, Te)$. As a result, they observed a significant power factor of 12.53 mW/m^2 at a temperature of 300 K [4]. However, in Petritis, D., et al. [10], the researchers published the TE characteristics of the selected chemicals based on First-Principles calculations. On the

other hand, the investigators of this research successfully estimated the lattice thermal conductivity while demonstrating significant differences in their TE characteristics when compared to the ones stated aforementioned. The world's energy scarcity and global warming problems have forced people to look for new ideas for generating effective and environmentally friendly technologies [12]. To serve as thermoelectric materials, Ta-series compounds have the necessary characteristics, including structural stability, low toxicity, and high potential. This investigation employs density functional theory (DFT) to investigate the structural, mechanical, electronic, thermodynamic, optical, as well as thermoelectric qualities of these compounds. Some of the important points, which are worthy of significant attention, are the values of their indirect band gaps and their manifested high thermoelectric efficiency [13, 14]. These materials have potential in a variety of fields, namely optoelectronic and photocatalytic materials, semitransparent electrodes, thermoelectric conversion devices, refrigeration appliances, and numerous energy-conserving devices [15]. Due to their varied competencies, they are suitable options for responding to both energy and environmental issues.

In the present study, the thermoelectric characteristics of Ta-series chemicals are presented by using first-principles computation in the framework of DFT computation. The main focus of this investigation is to characterize the physical attributes of the understudied materials. Using DFT, we demonstrate the AB_3X_4 compounds and investigate some of their substantial features, including structural, mechanical, electronic, thermodynamical, optical, as well as thermoelectric qualities. This section only provides the introduction of selected compounds, and the second section illustrates the methodology of our investigation. The third section primarily focuses on the results and briefly discusses the characteristics of understanding materials by using DFT approaches in the framework of Quantum Espresso. In the last section, we conclude our findings and summarize the discussion.

2 Computational Method

In the current investigation, the DFT computation were performed within the context of the quantum espresso (QE) algorithm [16, 17] in order to ascertain the physical qualities of the $TaCu_3X_4(X = S, Se, Te)$ chemicals. The Plane-Wave Basis-Set plus Pseudo-Potentials approach is implemented in all of the aforementioned computations [18]. The extrapolation of the wave-function within the framework of plane-wave as well as norm-conserving Pseudo-Potentials is used to get a description of the interactions that take place between the electrons along with the atomic core. The aforementioned methodology produces well-converged

information along with rapid electron–ion potential [19, 20], which indicates that the nucleus plus inner electrons of the ions operate as a core that valence electrons can interact with it. Initially, the process for structural relaxation was conducted by minimizing energy as well as internal forces in QE. This was accomplished by utilizing the generalized gradient approximation (GGA) [21] of the PBE function setting, the $3 \times 3 \times 3$ k-point and cutoff energy for wave functions that were greater than $50R_y$, the Projector-augmented plane-wave [22] Pseudo-Potential basis, the energy convergence threshold of $1 \times 10^{-07}R_y$, the force convergence threshold of $1 \times 10^{-03}R_y$, and the Marzari–Vanderbilt smearing [23] with a width of $0.002R_y$. In order to alloy via Se, one Te atom was substituted with a Se atom, and the structure was improved after a symmetrical arrangement was applied. Additionally, in order to decrease the stresses, the Hellmann–Feynman forces, which have a size of 0.005eV/Å, have been successfully implemented.

In order to facilitate quicker computations without compromising performance, the plane-wave pseudo-potential approach takes into consideration the orbital form in advance. The interaction between the electrons that reside in the outermost shell and the innermost ions of $TaCu_3X_4$ compounds is what determines the physical characteristics of the under study compound at the atomic level. There is no consideration given to any other electrons, including the electrons that make up the core. Therefore, it can be concluded that the behavior of under investigation compounds is attainable merely by utilizing the valence electron structure of the elements that make up it. In order to address exchange energies along with electronic exchange–correlation impacts, norm-conserving pseudo-potentials manufactured by employing the Troullier-Martins approach [20, 24] in combination with the PBE function [25, 26] were employed. Employing the Broyden-Fletcher Goldfarb Shanno (BFGS) technique [27], the crystal structure of aforementioned substances is optimized. For the objective of differentiating the core along with outermost levels and preventing the diffusion of charges from the core states, we selected substantial cutoff values of $50R_y$ and $645R_y$ for the wave-function plus charge density, correspondingly [28]. For structural relaxation, an automated $3 \times 3 \times 3$ k-point matrix is implemented; for DOS computations, a denser $9 \times 9 \times 9$ k-point grid utilized. In the first Brillouin Zone (BZ), electronic band structure computations are carried out along the high symmetrical k-path orientation (Γ-X-M-Γ-R-X-M-R). The Thermo-PW programming was utilized to determine the thermodynamical attributes. The BoltzTraP2 coding was used for estimating the thermoelectric qualities, with the QE software contributing to the calculation.

3 Results and Discussion

3.1 Structural Properties

In response to the findings of the optimization process for $TaCu_3X_4$(X = S, Se, Te) compounds that were under consideration, it has been determined that these materials have FCC cubic structures coupled with the space group P-43m [29]. These structures have X-atoms present at corner positions, and the Ta-atom is located at the body centered location. Cu-atoms are positioned in their middle of the edges. To find the numerical values of the variables, such as lattice constants, at the lowest possible state, we have optimized structural attributes by using the PBE-GGA method. The convergence of total energy determines how the internal components are evaluated [7]. Figure 1 depicts the optimization graphs of Ta-series chemicals and Table 1 lists the lattice parameters that has been computed. The outcomes shown in Table 2 indicate that the lattice constants $TaCu_3Te_4$ are much higher than $TaCu_3S_4$ and $TaCu_3Se_4$ materials. This may be a consequence of the fact that the atomic radius of Te-atom is greater than that of S-atom and Se-atom.

In the effort to determine the ideal relaxed structure, several calculations that include the variation of lattice constants and allow atoms to reduce the force between them until reaching a strict convergence threshold on forces have been performed [30]. The convergence criteria during the structural optimization process of Ta-series chemicals ensure the accuracy as well as reliability of their computed properties. Energy convergence means that the total change in energy between iterations must be less than 10^{-6} eV. Force convergence means that each atom's maximum force must be less than 0.00eV/Å. Stress convergence means that the maximum stress within the unit cell must be less than 0.02 GPa. And displacement convergence means that the atomic displacement between iterations must be less than 5×10^{-4}/Å. These stringent criteria guarantee precise structural optimization results. By accumulating total energies for each set of distinct lattice constants in Fig. 1a–c for $TaCu_3X_4$(X = S, Se, Te) compounds, we were able to depict total energy vs. volume as shown in Fig. 1. An important factor that needs to be taken into account while performing DFT computation is structural stability of the compound. Crystal structure stability is one of the important factors when we interested in using a compound for practical application. Regarding this, we acquired the binding energies (E_b) of $TaCu_3X_4$(X = S, Se, Te) compounds. The following relation can be employed to get E_b.

$$E_b = E_{total}^{TaCu_3X_4} - \left[E_{total}^{Ta} + 3E_{total}^{Cu} + 4E_{total}^{X=Se,Te,S} \right] \quad (1)$$
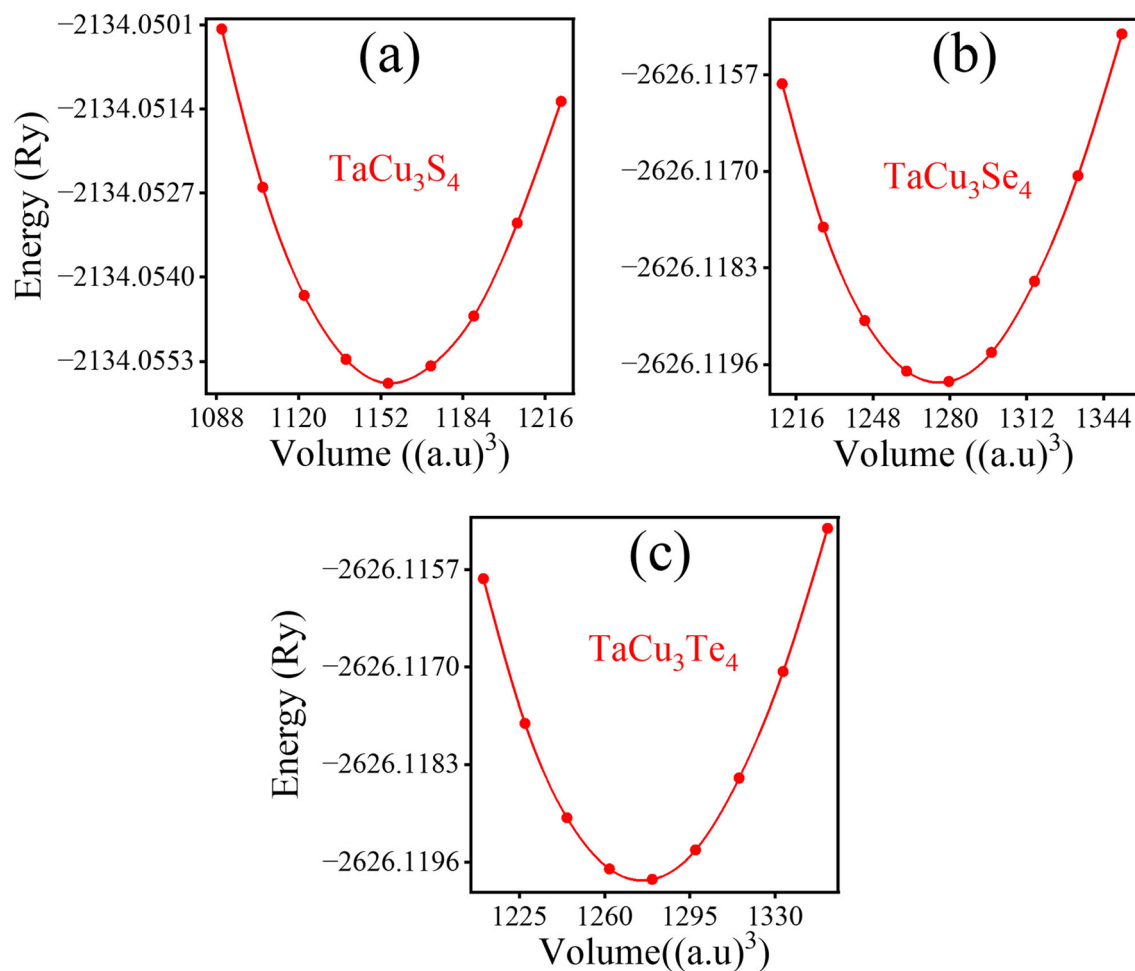
Fig. 1 The curves of optimization for $TaCu_3S_4$ (a), $TaCu_3Se_4$ (b), and $TaCu_3Te_4$ (c) compounds

Table 1 The table Summarizing Optimization Steps and Convergence Criteria

Step	Description	Convergence Criteria
Initial structure generation	Generate initial atomic positions and lattice parameters	N/A
Set convergence criteria	Define the criteria for energy, force, stress, and displacement	Energy: 10^{-6} eV Force: 0.01 eV/Å Stress: 0.02 GPa Displacement: 5×10^{-4} Å
SCF calculation	Perform self-consistent field calculations to determine electronic structure	N/A
Check convergence	Verify if energy, force, stress, and displacement criteria are met	Criteria defined above
Update Positions	Adjust atomic positions and lattice parameters if criteria are not met	N/A
Repeat SCF calculation	Continue the SCF calculations with updated positions until criteria are satisfied	Until all criter7ia are met
Save optimized structure	Save the final atomic positions and lattice parameters once optimization is complete	N/A

The ascertained values of the binding energies of the $TaCu_3S_4$, $TaCu_3Se_4$, and $TaCu_3Te_4$ compounds are −14317.8, −18705.5, and −26753.5 eV, respectively. The values of larger binding energy depict the stronger bonding within a material, which is frequently correlated with structural stability [31]. In the case of semiconducting materials, the structure stability is crucial for their functionality. The compound $TaCu_3Te_4$ have greater structural stability as compared to $TaCu_3S_4$, and $TaCu_3Se_4$

Table 2 The computed and optimized Lattice Parameter (a_0), Volume (V), Binding energy (E_b), and Band gaps (E_g) of $TaCu_3X_4$(X = S, Se, Te) compounds

Parameters	$TaCu_3S_4$	$TaCu_3Se_4$	$TaCu_3Te_4$
a_0 (Å)	5.552	5.745	6.009
V (Å^3)	611.147	677.123	774.826
E_b (eV)	− 14,317.844	− 18,705.590	− 26,753.538
E_g (eV)	1.71	1.60	1.15

compounds. Therefore, the studied compound is better candidate for optoelectronics and TE performance.

3.2 Mechanical Properties

The understanding of elastic attributes was an essential component in the process of elucidating the strength of crystalline materials [32]. In order to gain useful perspectives into the behavior of materials when exposed to mechanical as well as dynamic stresses, we have conducted an evaluation of the mechanical characteristics of $TaCu_3X_4$(X = S, Se, Te) compounds. In addition, these features have the highest significance when it comes to figuring out the strength of the crystal structure as well as the inherent cohesive qualities involved. It is essential to figure out the elastic constants of a substance in order to describe its crystal structure. This is commonly conducted by doing computations to figure out the total energy in the lowest energy level. By taking into consideration elastic stiffness constants, it has been possible to determine a number of elastic parameters for a variety of crystal structures [33, 34]. These parameters include Bulk-Modulus (B), Poisson ratio (B/G), specific heat capacity (C), along with melting states. The intrinsic variability of each crystal structure is illustrated by these elastic stiffness constants inside the crystal. There are three distinctive and autonomous stiffness constants that may be found in cubic $TaCu_3S_4$, $TaCu_3Se_4$, and $TaCu_3Te_4$ compounds. These constants are referred to as C_{11}, C_{12}, and C_{44}. To be more specific, C_{11} refers to the resistance that the material encounters while it is being deformed longitudinally, and C_{22} describes the features of the material when it is being expanded transversely. The constant C_{44} provides information about the material's hardness as well as its ability to withstand shear deformation because of the effect of shear strain that is imparted [35, 36].

In order to asses the mechanical stability of a substance, it is essential that the stiffness constants (C_{ij}) correspond to the Born-Stability criteria [37, 38]. A representation of this requirement may be found in Eq. (3), which can be expressed as follows:

Table 3 According to the estimated outcomes of the stiffness equation for $TaCu_3X_4$(X = S, Se, Te), the following parameters are included in the equation: Elastic constants are denoted by the symbol C_{ij}, whereas elastic moduli are represented by B, G, and Y. Furthermore, the Cauchy-Pressure, the Pugh-ratio, the Poisson-ratio, and the shear constant have been included as well:

Parameters	$TaCu_3S_4$	$TaCu_3Se_4$	$TaCu_3Te_4$
C_{11} (GPa)	91.314508	72.171159	60.263125
C_{12} (GPa)	12.979171	13.939331	19.104022
C_{44} (GPa)	19.523705	20.211251	20.906672
B (GPa)	39.09	33.34	32.82
G (GPa)	25.90	23.40	20.77
γ (GPa)	63.61	56.89	51.46
B/G	1.50	1.42	1.58
G/B	0.66	0.70	0.63
υ	0.22	0.21	0.23
C_P (GPa)	− 6.54	− 6.27	− 1.80
A	0.49	0.69	1.01

$$\begin{cases} (C_{11} - C_{12}) > 0 \\ C_{11} > 0; C_{44} > 0 \\ (2C_{12} + C_{11}) > 0 \end{cases} \tag{2}$$

The Table 3 illustrate the calculated elastic constants for $TaCu_3X_4$(X = S, Se, Te) compounds. The results of this calculation indicate that $TaCu_3S_4$, $TaCu_3Se_4$, and $TaCu_3Te_4$ chemicals are stable, since they satisfy the stability-criterion stated in Eq. (1). They are also stable. In order to figure out the precise elastic-stiffness constants, especially C_{11}, C_{12}, and C_{44}, a variety of approximations are used. These approximations include the Reuss [39], Voigt [40], and Hill [41] approaches. Because of the complex relationship that exists between strain and stress in calculating these constants, these procedures are very necessary. In order to show the lower along with upper bounds for the Bulk-modulus, respectively, the Reuss along with Voigt approaches are employed. This is accomplished by presuming that the values of stress and strain are homogeneous across the entire grains. On the other hand, the Hill approach, which is an intersection of the Reuss & Voigt approaches, shows findings that demonstrate a higher degree of consistency with the discovery made via observation [42, 43].

The Reuss, Hill, and Voigt approaches, which are illustrated by Eqs. (3) and (4) [44, 45], which may be used to compute the bulk moduli (B), are as follows:

$$B = B_R = B_V = \frac{1}{3} \times (C_{11} + 2C_{12}) \tag{3}$$

$$B_H = \frac{1}{2} \times (B_v + B_R) \tag{4}$$

By using Eqs. (5), (6), and (7), respectively, one may determine the Reuss shear (G_R), the Hill shear [(G_H)], and the Voigt shear [(G_V)] moduli, respectively.

$$G_R = \frac{5(C_{11} - C_{12})C_{44}}{4C_{44} + 3(C_{11} - C_{12})} \tag{5}$$

$$G_H = \frac{1}{2} \times (G_v + G_R) \tag{6}$$

$$G_v = \frac{1}{5}(C_{11} + 3C_{44} - C_{12}) \tag{7}$$

In order to determine further critical parameters, we only depend on the results obtained from the Hill approach. These parameters include the young modulus (γ), the anisotropy factor (A), as well as the Poisson ratio [46].

$$\gamma = \frac{9BG}{G + 3B} \tag{8}$$

$$A = 2 \times \frac{C_{44}}{(C_{11} - C_{12})} \tag{9}$$

$$\upsilon = \frac{3B - 2G}{2(G + 3B)} \tag{10}$$

B is a measurement that provides substantial information on the bond strength of a substance [53]. It performs as a measurement of the elasticity along with incompressibility of a substance, as well as its link to the substance's resistance to employed stress. When modifications take place inside the cubic structure of $TaCu_3X_4(X = S, Se, Te)$ compounds, the findings that are reported in Table 4 reveal a considerable drop. Among the compounds, $TaCu_3S_4$ has the greatest value of B, which indicates that it has a large resistance to changes in its volume. Furthermore, the shear modulus (G) is applied to assess the chemical's ability to tolerate deformation brought on by shear stress throughout the process of shear stress. The elastic modulus, also known as G, is widely acknowledged in the sector due to the fact that it provides a more in-depth comprehension of the rigidity of a substance

[54]. The compound $TaCu_3S_4$ has a higher value of G, which indicates that it possesses a higher degree of hardness compared to $TaCu_3Se_4$ and $TaCu_3Te_4$ compounds. Furthermore, it reveals a high degree of resistance to deformation.

In order to define the stiffness of the material, the parameter γ is employed. A greater value of γ indicates a higher degree of stiffness with respect to the substance. The current discussion provides an illustration of the γ, stiffness, and compressive resistance of a material while maintaining its distinctive characteristics. This is accomplished within the restrictions of the material's elastic constraints when the discussion is conducted. The data that pertain to γ, which are presented in Table 4 for $TaCu_3X_4(X = S, Se, Te)$ compounds, reveal that $TaCu_3S_4$ demonstrates a higher degree of stiffness in comparison to the other compound. This assertion is supported by the results that were acquired from the G findings. The B/G ratio, which is also referred to as the Pugh ratio, is a useful indication that may be used to determine whether a crystalline material is more susceptible to brittleness or ductility. The investigation of the relationship between the fracture resistance (indicated as B) as well as the deformation resistances (indicated as G) is represented by the B/G ratio.

In order to determine whether a material is brittle or ductile, we use the following scenario [47]. In the event that the B/G ratio is larger than 1.75, it is predictive of the ductile character of the material. Conversely, if the ratio is less than 1.75, it is indicative of the brittle nature of the material. Therefore, in our present scenario, $TaCu_3S_4$, $TaCu_3Se_4$, and $TaCu_3Te_4$ compounds are brittle. Furthermore, to determine the Pugh ratio, the parameter υ is of great significance since it is used to evaluate the brittleness or ductility properties with which a material is associated. When the υ is less than 0.33, it is characterized as brittle nature of the material, while materials with the σ value more than 0.33 demonstrate ductile nature of the material. Additionally, the letter υ is used to signify the measurement of the phenomena of contraction or expansion, which occurs in a direction that is opposite to that of axial strain. The presence of covalent bonding is indicated by a value of υ that is close to 0.1, while the presence of ionic character is indicated by a value that is equal to or more than 0.25 [19]. In the current scenario, the calculated values for $TaCu_3X_4(X = S, Se, Te)$ compounds are less than 0.33, which indicate that the compounds under study have brittle nature as well as bonding characteristics.

One important parameter that is employed to analyze a chemicals's ductility or brittleness is known as the Cauchy pressure (C_P). The differ between two distinct elastic-constants, C_{22} and C_{44}, must be employed to calculate the elastic constant C_P, which is written as ($C_P = C_{44} - C_{44}$). A material's brittleness or ductility can also be determined by employing the findings of C_P [57]. In Table 4, the computed C_P values for $TaCu_3X_4(X = S, Se, Te)$ compounds

Table 4 The computed findings of Debye temperature (θ_D), density (ρ), melting temperature (T_m), and average wave velocity (υ_m) for $TaCu_3X_4(X = S, Se, Te)$ compounds

Parameters	$TaCu_3S_4$	$TaCu_3Se_4$	$TaCu_3Te_4$
υ_m (m/s)	2529.838	2169.139	1948.583
ρ (g/cm^3)	4.84	6.02	6.72
θ_D (K)	271.238	225.113	192.859
T_m (K)	629.71 ± 300	635.39 ± 300	665.92 ± 300

are listed. The C_P findings shows that our compounds are brittle, as shown by their negative signs. The findings obtained pertaining to the previously specified mechanical parameters illustrate an outstanding degree of consistency, hence signifying the accuracy of our conclusions and confirming the validity of the technique utilised in our investigation. Moreover, in order to assess the elastic constants in various directions, it is important to take into account the anisotropic factor, which is denoted by A. In addition, the A parameter plays an important function in defining the features of fractures and deformation in a compound. The value of A is equal to one indicate that the compounds are isotropic whereas for anisotropic compound. Our findings given in Table 4 show that the compounds $TaCu_3S_4$ and $TaCu_3Se_4$ are anisotropic and the compound $TaCu_3Te_4$ is isotropic due to A is greater than one (A > 1).

The thermodynamical parameters of a compound including the Debye temperature (θ_D), which is used in the computation of thermal expansion, C, as well as melting-state, have an impact on the mechanical attributes of the compound by influencing its mechanical characteristics [48]. The phenomena that are being considered has a connection to the intrinsic frequency of elastic oscillations inside the lattice-profile. This frequency is obtained from the average velocity of elastic-waves, which is denoted by the symbol v_m. The determination of the θ_D for $TaCu_3X_4 (X = S, Se, Te)$ compounds may be accomplished by using Anderson's formulation, which incorporates the Vogit-Reuss approach [49].

$$\theta_D = \frac{h}{k_B}\left(\rho\frac{N_A}{M}\times\frac{3n}{4\pi}\right)^{\frac{1}{3}}v_m \tag{11}$$

The equation incorporate the Avogadro number which is denoted by N_A, the molecular weight is denoted by M, plank's constant is represented by h, Boltzmann constant is represented by k_B, the total number of atoms in the molecule is denoted by n [48, 50]. Through the application of the Eq. (10), it is also possible to articulate the average sound velocity v_m as a function of the transverse as well as longitudinal wave velocities.

$$v_m = \left[\frac{1}{3}\left(\frac{2}{v_l^3}+\frac{1}{v_t^3}\right)\right]^{-\frac{1}{3}} \tag{12}$$

In order to determine the values of v_t and v_l, it is possible to use the B as well as G figures, which are highlighted in Eqs. (12) and (13) respectively.

$$v_t = \left(G/\rho\right)^{\frac{1}{2}} \tag{13}$$

$$v_l = \left(\frac{4G + 3B}{\rho}\right)^{\frac{1}{2}} \tag{14}$$

The computed findings of v_m, ρ and θ_D for Ta-series compounds that were under study are shown in Table 4. According to the findings shown in Table 4, it can be seen that the value of θ_D for $TaCu_3S_4$ compound is larger than $TaCu_3Se_4$ and $TaCu_3Te_4$ compounds. It may be inferred from these findings that $TaCu_3S_4$ illustrates a higher degree of thermal conductivity when compared to $TaCu_3Se_4$ and $TaCu_3Te_4$ compounds. In addition to compute the melting temperature (T_m) of under studying compounds, we implement the Eq. (15).

$$T_m = \left[5.911C_{12} + 553(K)\right]\pm 300K \tag{15}$$

In Table 5, the anticipated values of $T_m(K)$ for $TaCu_3X_4 (X = S, Se, Te)$ compounds that are the focus of the investigation are addressed. For the $TaCu_3Te_4$ compound, the $T_m(K)$ values are greater than $TaCu_3S_4$ and $TaCu_3Se_4$ compounds, which indicates that the $TaCu_3Te_4$ compound has the best candidate in TE application that can be implemented at high melting temperature.

3.3 Electronic Properties

The study of the behavior of electrons in substances comprehensively is crucial for understanding the entire structure of compounds [51]. It is possible to identify the transitions of electrons between the lowest energy state of the conduction band along with the highest energy state of the valence band (VB) by analyzing the electronic band-structure attribute of a compound [14]. The current portion thoroughly examined the electronic attributes of the $TaCu_3X_4 (X = S, Se, Te)$

Table 5 The comparison of our calculated, previous calculated and experimental values of elastic constants (C_{ij})

| Compounds	Our Cal. Elastic Const			Pervious Cal. Elastic Const [29]		
	C_{11}	C_{12}	C_{44}	C_{11}	C_{12}	C_{44}
$TaCu_3S_4$	91	12	19	91	14	18
$TaCu_3Se_4$	72	13	20	71	13	17
$TaCu_3Te_4$	60	19	20	56	15	19

chemicals. The band structure profile of the under study compounds is depicted in Fig. 2. This profile has been calculated by using PBE-GGA approach in the higher symmetric k-path orientation (Γ-X-M-Γ-R-X-M-R) of the first BZ. As a result of their tendency to underestimate the intrinsic band gap in insulators along with semiconductors,

Generalized-Gradient-Approximation (GGA) approaches have attained notoriety through their application [52, 53]. Figure 3 depicts that each band structure illustration contains a dashed blue line that represents the level of Fermi energy (E_f), which is adjusted to zero. When considering the attributes of a material, the location of E_f is of the utmost
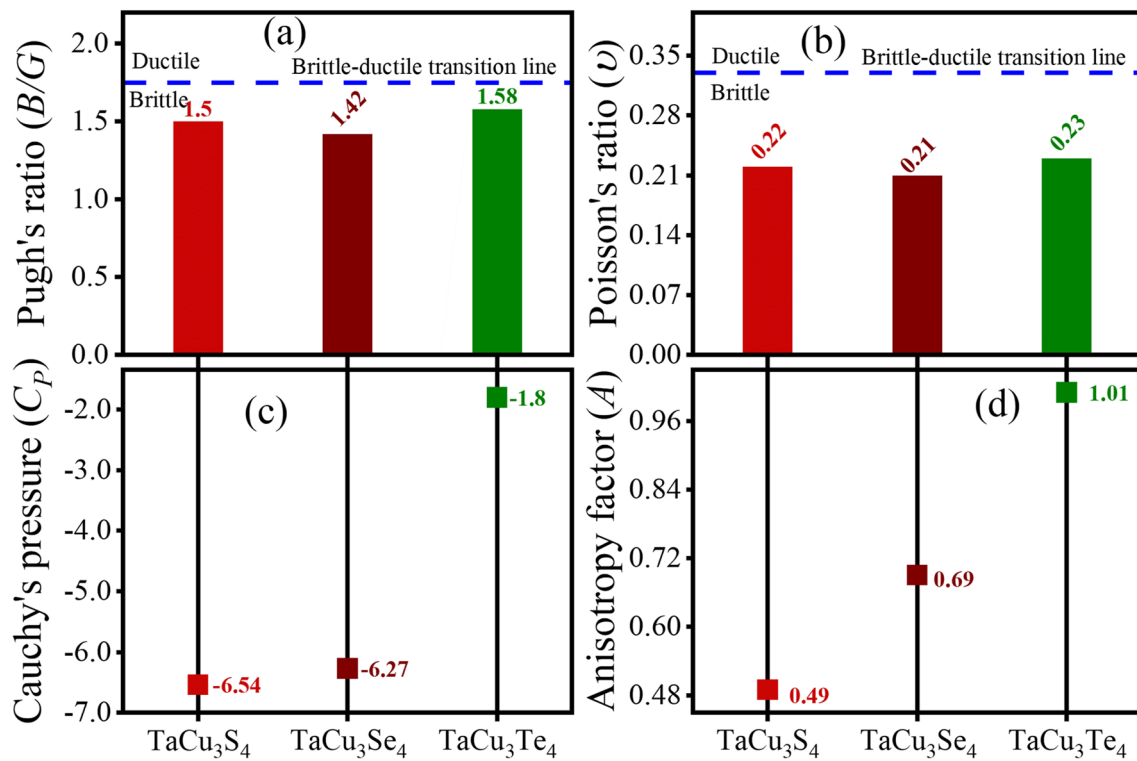
Fig. 2 The computed findings of Cauchy's pressure (C_P), Anisotropy factor (A), Poisson's ratio (v) and Pugh's ratio (B/G) for $TaCu_3X_4(X = S, Se, Te)$

**Fig. 3** The calculated band structure for $TaCu_3X_4(X = S, Se, Te)$ materials
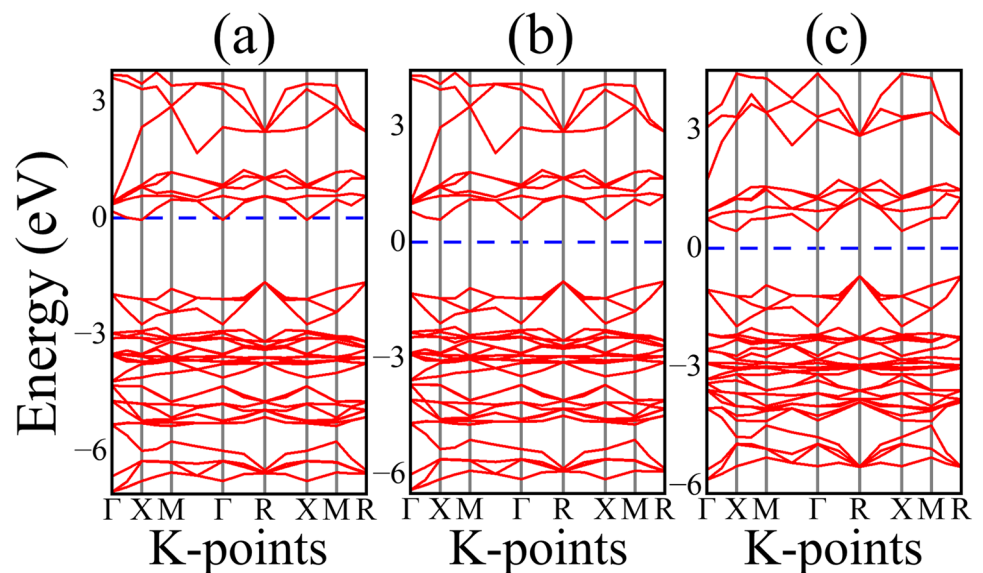
importance. A broad spectrum of material characteristics, such as magnetic, optical, as well as electrical capabilities, are strongly linked to the location of E_f within the band.

The band structures of the $TaCu_3X_4(X = S, Se, Te)$ compounds are illustrated in Fig. 3a–c, respectively. The indirect band gap (BG) of 1.71 eV for the $TaCu_3S_4$ compound is in close consistent with previous investigations [31, 54, 55], since the VBM along with CBM are positioned near the extremely higher symmetric points of R and Γ. Furthermore, the indirect BG for $TaCu_3Se_4$ and $TaCu_3Te_4$ compounds are 1.60 and 1.15 eV, which is an effective collaboration with earlier study [31, 54, 55]. In the ref. [31], the $TaCu_3S_4$, which also has an indirect band gap findings of 1.65 eV, is a compound that is comparable to under studied materials. Our computation predicts a well consistency to

the previously experiment calculated data [31, 54, 55]. As a result of the broadening of the band gap in understudied substances, its characteritics are comparable to those of semiconducting compounds. This makes studied materials an ideal choice for applications related to the electronic sector, such as optoelectronics and strain sensor technology [56], which need a band gap that vary between $0.1 − 3$ eV [57].

In order to have a better understanding of the band structures (BS), we have computed the total density of state (TDOS) as well as the partial density of state (PDOS) through the application of the PBE-GGA approach, which is shown in Fig. 4. In Fig. 4a–f, the plots of PDOS and TDOS offer a graphical depiction of the contributions that the electronic states make to the valence band (VB) along with the conduction band (CB). The information on the contribution
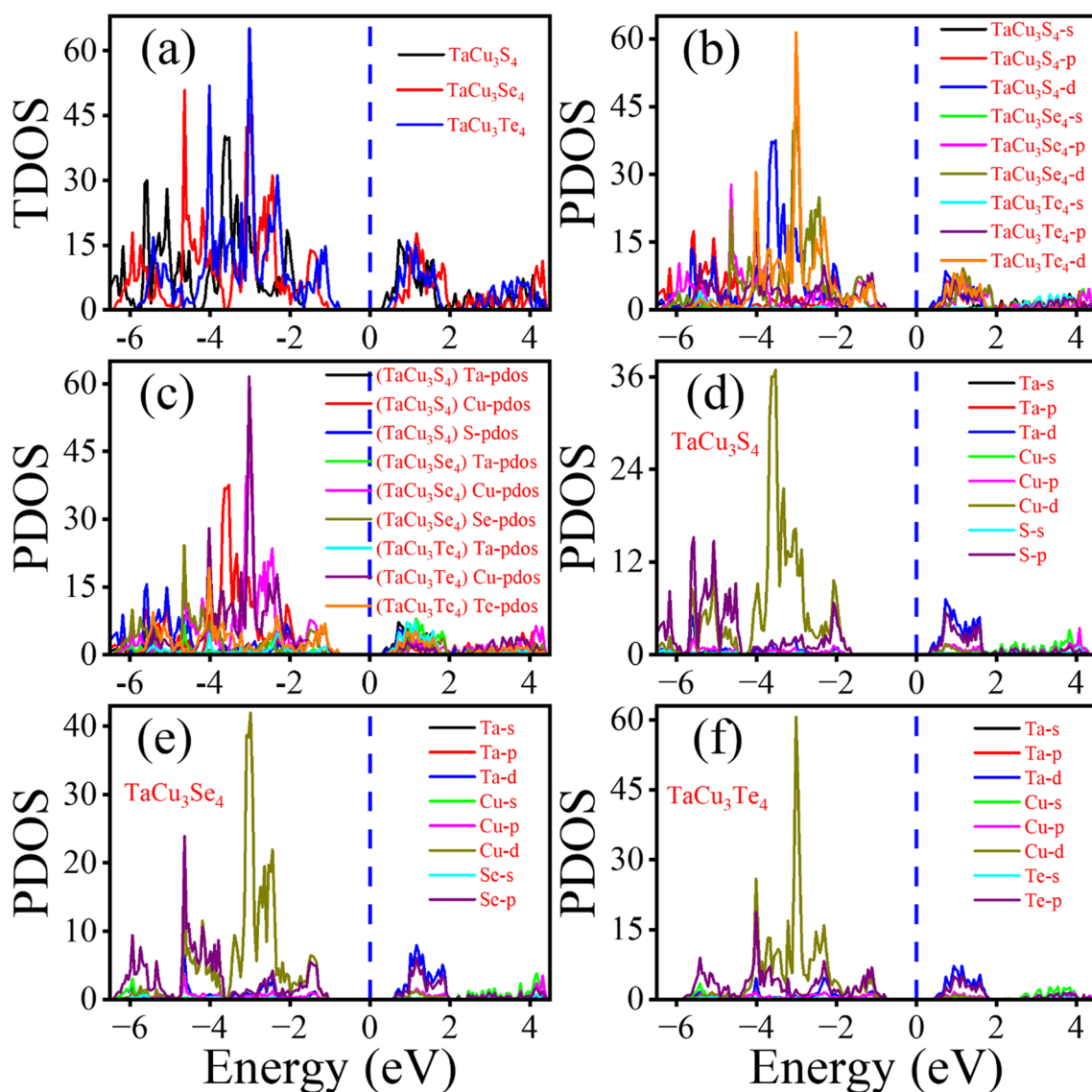
Fig. 4 Computed total density of state (TDOS) along with partial density of state (PDOS) for $TaCu_3X_4(X = S, Se, Te)$ compounds

of each sub-shell (s, p, and d) to the establishment of the band-structure is provided by the PDOS graphs. In the Fig. 4a, the plot display the TDOS of the selected chemicals. The plot shows the $TaCu_3Te_4$ compound give significant contribution in the VB and little enrollment in the CB. The valence band in the energy range of -4.8 to -2.3 eV is primarily occupied by Te-atoms, as Fig. 4b illustrates. Due to the presence of a significant peak of Te-atoms at the E_f level, it is evident that Te-atoms play an integral function in the creation of band-structure along with having an influence for the conductivity of the compounds. Additionally, the p-states of Te-atoms exhibit significant allocation in the valence band and just a little presence in the conduction band, in contrast to the d-states of Ta-atoms, which exhibit little contribution both in the valence along with conduction bands. In the valence and conduction bands, the p-states of Cu-atoms and the s-states of the involved atoms also make a little contribution. Our band structure profile is consistent to previous study [58, 59].

A visual representation of the anticipated PDOS for $TaCu_3X_4(X = S, Se, Te)$ materials are shown in Fig. 4b–f. These PDOS provide valuable understanding into the electronic band-structures, facilitating comprehension and decoding. A visual depiction of the contributions that the electronic states make to the valence VB and the CB [60] is presented by the graphical representations of PDOS. Figure 4d indicates that for $TaCu_3S_4$, the d-states of Cu-atoms and s-states of S-atoms are mostly responsible for the formation of the CB. Conversely, the d-states of Ta-atoms and the s-states of S-atoms primarily contribute to the creation of the VB. On the contrary, in the scenario of the $TaCu_3Se_4$ and $TaCu_3Te_4$ compounds, the d-states of Cu-atoms and s-states of Se-atoms contribute substantially to CB, but the d-states of Ta-atoms and s-states of Se-atoms are less contributed to VB in Fig. 4e, f. In conclusion, $TaCu_3X_4(X = S, Se, Te)$ compounds are a strong candidate for use in optoelectronic technology due to its advantageous band gap and effective electrical characteristics [57].

3.4 Thermodynamical Properties

The thermal stability of the compound illustrated by analyzing the thermodynamic characteristics of Ta-series compounds by the application of first-principle calculations. At the lowest possible state of pressure (0 GPa), the thermodynamic characteristics of $TaCu_3X_4(X = S, Se, Te)$ compounds were established. The thermodynamic attributes of under investigated compounds at temperature ranges between 0 and 800 K are shown in Fig. 5. Figure 5a–d illustrate how vibrational energy ($E_{vib.}$), Debye entropy (ΔS), vibrational free energy (E_{free}), and Debye heat capacity (C_D) of compounds vary with temperature. The circumstances of zero pressure are taken into account in the calculation to figure out the search query's variables. The graphical representations illustrate that the findings of E_{free} for $TaCu_3X_4(X = S, Se, Te)$ compounds are approaching to zero as the temperature falls below 100 K. This results in an equivalent rise in $E_{vib,}$, C_D, and ΔS when temperature increases, while the findings of E_{free} experiences fall as the temperature raise up. As Fig. 5a shows, the linearity of the $E_{vib,}$ function of $TaCu_3X_4(X = S, Se, Te)$ has an optimal finding of 160.35 eV at 800 K, demonstrating the material's magnificence.

The A value in the negative range of the E_{free} may be used to characterize the thermodynamic stability of any material, according to investigation [61]. Consequently, the thermodynamic stability of under studying compounds has been shown in Fig. 6b. The maximum value of the examined vibrational free energy for $TaCu_3S_4$, $TaCu_3Se_4$, and $TaCu_3Te_4$ at 800 K, is found to be -254.79 eV, -224.94 eV, and -277.89 eV, respectively. Furthermore, comprehension of the thermal energy of a system may be obtained from the concept of entropy. It is specifically calculated that while the temperature persists at zero kelvin (0K), the entropy is zero. A phenomenon called thermal-expansion exits as the temperature of a compound increase. As a result of the aforementioned procedure, the material's volume increases concurrently. The phenomena might be explained by the idea that as temperature rises, atomic particle thermal vibrations intensify and become increasingly perceptible. As seen in Fig. 6c, when $TaCu_3S_4$, $TaCu_3Se_4$, and $TaCu_3Te_4$ is subjected to heat at 800 K, the energy levels at which the highest value of entropy may be reached are 481.47 eV, 517.74 eV, and 548.48 eV, respectively.

The findings that were reported earlier show that the $TaCu_3X_4(X = S, Se, Te)$, has a greater degree of thermodynamic stability, as well as is suited for a broader spectrum of applications across a number of fields. To be more explicit, the C_v is a thermodynamic stability that characterize the amount of heat that is absorbed or expelled by a material when its T(K) rises or falls by a factor of one (1K). The visual representation of the relationship between C_v and temperature can be seen in Fig. 5d, which illustrates the connection that exists between the two variables concerned. It is possible that other phenomena, such as electronic degrees of freedom and harmonic impacts, are responsible for the decrease in the slopes of heat-capacities of $TaCu_3X_4(X = S, Se, Te)$ compounds have a heat capacity of 198.93 eV at a temperature of 800 K. This decline in C may be attributed to the lowering slopes. It should not come as a surprise that the behavior that is anticipated by Dulong-Petit's [62] rule for C_v corresponds with that conclusion.
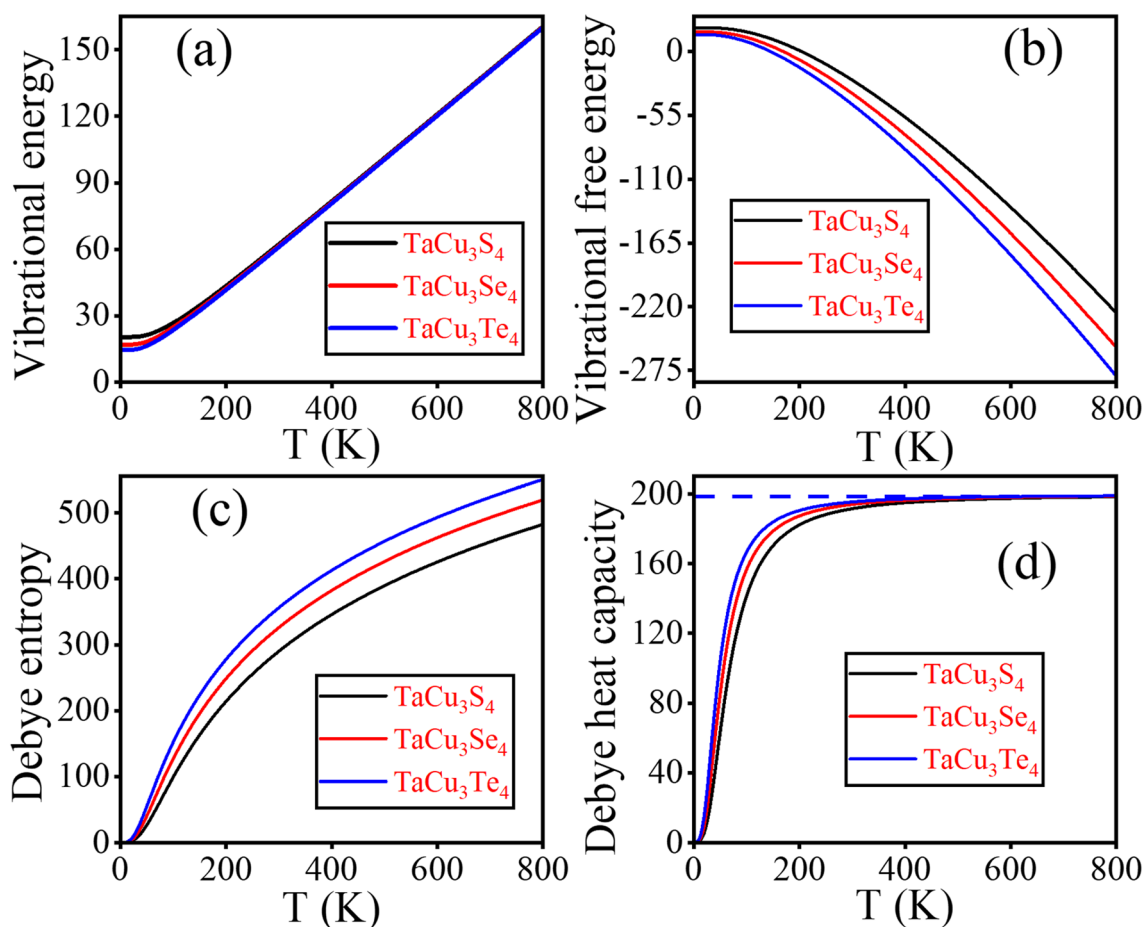
Fig. 5 The variation in TaCu$_3$X$_4$(X = S, Se, Te) compounds volume per unit of cell under different pressure and temperature conditions throughout the experiment

3.5 Optical Properties

The behavior of the substance has been researched by means of the interaction of a highly energetic photon beam, offering significant knowledge for its prospective uses in various aspects of photovoltaic studies. In the present sections, we will introduce the different optical attributes that are associated with TaCu$_3$X$_4$(X = S, Se, Te) compounds.

3.5.1 Dielectric Function

A substanc's ability to store electrical power in an electric field is ascertained by its dielectric constant, or ε(ω). This pertains to capacitive uses electronics along with the polarization response of a substance to an external field that modifies its insulation [54]. There are many optical characteristics that may be described by utilizing the dielectric function [ε(ω)], as well as these optical qualities are also associated with optimum lattice constants [57, 63–66]. One of the components of the ε(ω) is real, denoted as $\varepsilon_1(\omega)$, whereas the other component is imaginary, denoted as $\varepsilon_2(\omega)$. Both are connected to one another by following relation.

$$\varepsilon(\omega) = \varepsilon_1(\omega) + i\varepsilon_2(\omega) \tag{16}$$

$$\varepsilon_1(\omega) = 1 + \frac{\pi}{2}P \times \left(\int_0^\infty \frac{\omega'\varepsilon_1(\omega')}{\omega'^2 - \omega^2} \right) d\omega' \tag{17}$$

$$\varepsilon_2(\omega) = \frac{4\pi^2 e^2}{\Omega} \lim_{q \to 0} \sum_{c,v,k} w_k \delta\left(\in_{ck} - \in_{vk} -w \right)$$
$$\times \left(\langle u_{ck} + e_{\alpha q} | u_{vk} \rangle \langle u_{ck} + e_{\alpha q} | u_{vk} \rangle^* \right) \tag{18}$$

The material's polarization is dictated by $\varepsilon_1(\omega)$, whereas the absorption (loss or gain) is dictated by $\varepsilon_2(\omega)$ dielectric function [66]. The spectrum of $\varepsilon_1(\omega)$ and $\varepsilon_2(\omega)$ for TaCu$_3$X$_4$(X = S, Se, Te) stable compounds are indicated in Fig. 6a, b, respectively. In the region of energy from $0 - 10$ eV, the spectrum of under investigated compounds have been characterized. Within the aforementioned energy
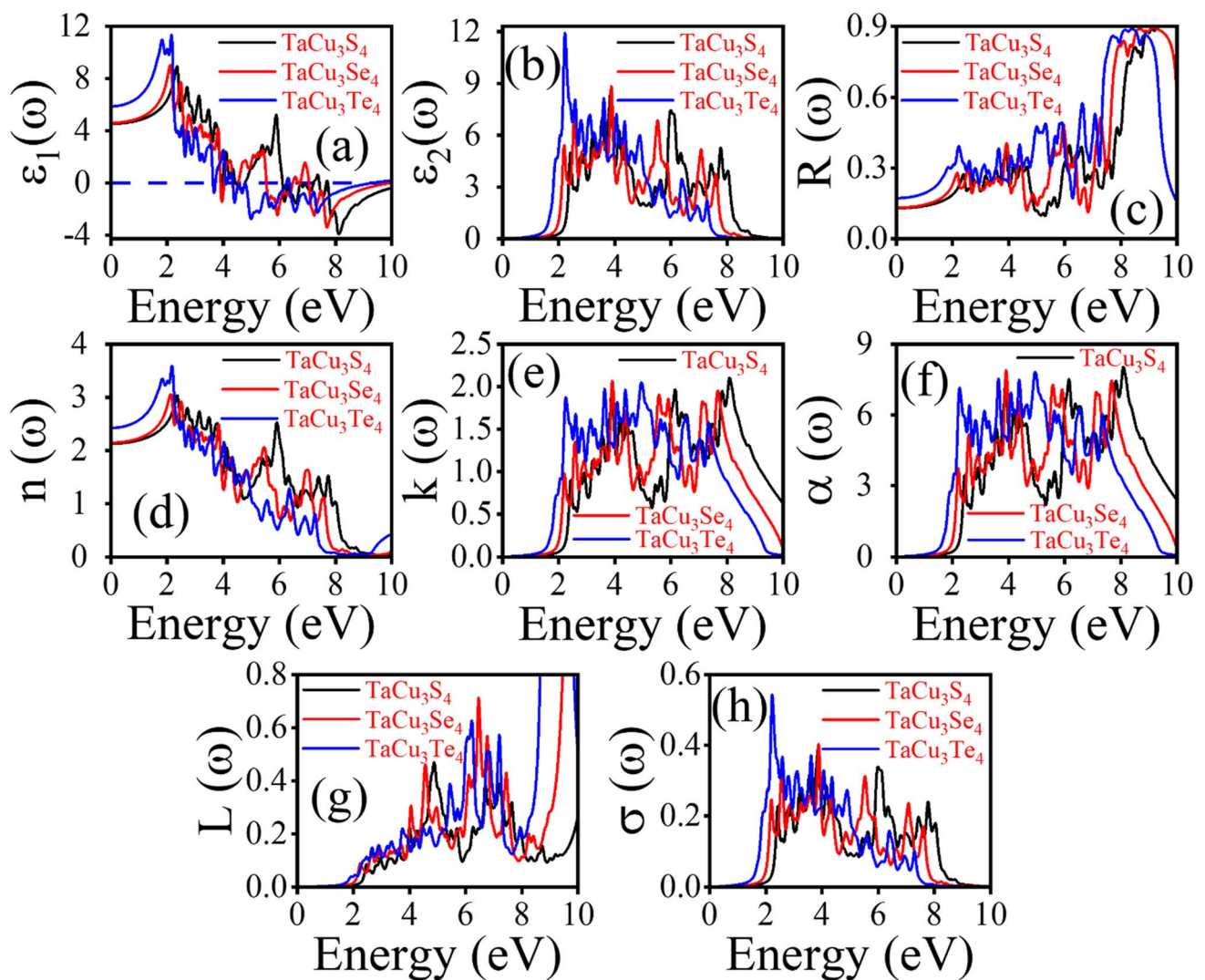
Fig. 6 Estimated optical attributes for the $TaCu_3X_4$(X = S, Se, Te) compounds

range, the real dielectric constant is responsible for characterizing the dissipation of energy as well as the damping effect of the waves. Figure 6a displays the value of $\varepsilon_1(0)$, or the static dielectric constant, for $TaCu_3X_4$(X = S, Se, Te) materials. It indicates that the $TaCu_3Te_4$ compound has a projected value of $\varepsilon_1(0)$ is 5.87, whereas the $TaCu_3S_4$ and $TaCu_3Se_4$ compounds have a projected value of $\varepsilon_1(0)$ are 4.54 and 4.59. This indicates that the $TaCu_3Te_4$ compound dissipates more energy than the other both compounds. From the perspective of the pen model, a material is said to have a large band gap if it has a lower figure of the static dielectric constant. Therefore, it is projected that the $TaCu_3Te_4$ compound would have a smaller band-gap energy reading in comparison to the $TaCu_3S_4$ and $TaCu_3Se_4$ compounds.

Surprisingly, the illustration of electronic band structure shown in Fig. 3 indicates that the under investigated stable compounds correspond to the pen model. For $TaCu_3S_4$,

$TaCu_3Se_4$, and $TaCu_3Te_4$ compounds, the maximum peak of $\varepsilon_1(\omega)$ is 8.94, 9.50, and 11.34, respectively, located at 2.35, 2.20 and 2.15 eV (UV area). Furthermore, as shown in Fig. 6a, there is a significant energy dissipation in $TaCu_3X_4$(X = S, Se, Te) materials for low photon energy values, and this behavior persists at increasing photon energy values. The initial critical point for the aforementioned substances may be located at 0 eV in Fig. 6b. Surprisingly, $TaCu_3Te_4$ has 5.01% greater absorptive power than $TaCu_3S_4$, and $TaCu_3Se_4$ compounds.

3.5.2 Reflectivity

The reflecting coefficient, also known as Reflectivity $R(\omega)$, is examined in order to evaluate the efficiency of the substance that is being investigated. The amount that the substance bounces the incoming light is indicated by the symbol R(ω).

The use of critical coatings is necessary for devices that need low energy reflection loss. Examples of such devices are lenses, mirrors, optical as well as solar systems [67]. The coefficient in question reflects the fraction of the incident light that bounces back upon hitting the surface of the substance. The relation was employed to ascertain the $R(\omega)$ of studied compounds.

$$R(\omega) = \left| \frac{\sqrt{\varepsilon_1(\omega) + i\varepsilon_2(\omega)} - 1}{\sqrt{\varepsilon_1(\omega) + i\varepsilon_2(\omega)} + 1} \right|^2 \quad (19)$$

Figure 6c offers a visual representation of the spectrum of $R(\omega)$ for $TaCu_3X_4(X = S, Se, Te)$ compounds, which have been displayed. It is important to note that the strongest reflections take place at photon energy states where the degree of absorption has approached its lowest value. In the case of $TaCu_3S_4$, $TaCu_3Se_4$, and $TaCu_3Te_4$ compounds, the static figures of reflectivity ($R(0)$) are 0.13, 0.14, and 0.17, respectively. The $R(0)$ increases with energy to approach its maximum value of 0.88, 0.89, 0.89 occurring at 8.84, 8.66, and 8.39, respectively. As ranges of energy meet the energy of the band gap, the substance's reflectivity decreases and its opacity to incoming photons is increased. These findings demonstrate the Ta-based compounds are suitable in the application of PV technology and lenses because of their opacity in this lower energy gap.

3.5.3 Index of Refraction

The index of refraction which is donated as $n(\omega)$ is employed to measure a material's openness. The $n(\omega)$ spectrum is implemented to ascertain the degree of transparency of a specimen towards incident light rays. In order to describe the behavior in which light travels through a substance, the $n(\omega)$ is used. This is because it alters the speed and direction of light. It is essential for controlling light and guaranteeing efficient transmission in lens design, fiber optic cables, and other equipment [55]. The $n(\omega)$ can be computed by following relation.

$$n(\omega) = \sqrt{\frac{\left[(\varepsilon_1(\omega))^2 + (\varepsilon_2(\omega))^2 \right]^{1/2}}{2} + \frac{\varepsilon_1(\omega)}{2}} \quad (20)$$

The $n(\omega)$ profiles for the stable compounds under investigation are shown in Fig. 6d. For the $TaCu_3S_4$, $TaCu_3Se_4$, and $TaCu_3Te_4$ compounds, the static refractive indices are 2.13, 2.14, and 2.42, respectively. According to the $n(\omega)$ visualization, it is evident that understudied compounds exhibit low refractivity readings in the less energetic-zone. Furthermore, this figure presents an upward trend as the energy level rises, ultimately reaching its maximum level. The compounds $TaCu_3S_4$, $TaCu_3Se_4$, and $TaCu_3Te_4$ have the maximum figures of $n(\omega)$ at 2.37, 2.14, and 2.17 eV, respectively.

3.5.4 Extinction Coefficient

The extinction coefficient, denoted by the symbol $k(\omega)$, provides an explanation for the magnitude and nature of the electromagnetic radiation that is absorbed by a particular substance [68]. The extinction coefficient is a measure that reflects the amount of light that has been "attenuated" in terms of the wave degeneration that occurs as a result of radiation being absorbed and scattered. For photodetectors along with solar cells that absorb and transform light energy, significant values indicate higher light absorption qualities [54]. Furthermore, the absorptive capacity and efficiency of a material are described by the $k(\omega)$ spectra. The subsequent equation provides an alternative way to express the $k(\omega)$: as $\varepsilon(\omega)$.

$$k(\omega) = \frac{1}{\sqrt{2}} \times \sqrt{\frac{\left((\varepsilon_1(\omega))^2 + (\varepsilon_2(\omega))^2 \right)^{\frac{1}{2}}}{2} - \varepsilon_1(\omega)} \quad (21)$$

The $k(\omega)$ spectra of the $TaCu_3X_4(X = S, Se, Te)$ compounds are shown in Fig. 6e. Furthermore, the $TaCu_3S_4$, $TaCu_3Se_4$, and $TaCu_3Te_4$ compounds display a peak value of $k(\omega)$ are 2.01, 2.06, and 2.04, which takes place at an energy level of 8.09, 3.90, and 4.96 eV, respectively. By comparison, the compound $TaCu_3S_4$ has a maximum $k(\omega)$ figure of 2.06, which is measured at an energy level of 3.90 eV.

3.5.5 Absorption-Coefficient

The absorption coefficient, designated $\propto(\omega)$, is an indicator of the ability of the substance to absorb light, depending on the path's length. This is especially true because, for instance, in applications such as photovoltaic cells, the yield relies on the efficiency of a substance in converting light into power [13]. Moreover, it clarifies the ability of substance to convert solar energy. The present research also clarifies a substance's ability to permit the penetration of a certain electromagnetic radiation. The subsequent equation can be used to calculate $\alpha(\omega)$.

$$\alpha(\omega) = \frac{2k}{c}\omega = \frac{4\pi}{\lambda}k \quad (22)$$

The graphical profile of $\alpha(\omega)$ for Ta-series compounds is shown in Fig. 6f. The $TaCu_3X_4(X = S, Se, Te)$ compounds show significant absorption in the energy range of $2.25 - 8.09$ eV, as indicated by the several peaks present in the $\alpha(\omega)$ spectra. Absorption decreases until it approaches 10 eV, which is the point at which it peaks at its maximum figures. The term "threshold point" describes the point at which a substance appears to absorb electromagnetic radiation. The graph that illustrates this phenomenon reveals that

the compounds under investigation have a threshold point that is located at $1.52eV$. By illustration of the $\alpha(\omega)$ figure, the $TaCu_3S_4$, $TaCu_3Se_4$, and $TaCu_3Te_4$ materials exhibit significant peaks are 7.82, 7.89, and 7.82 occurred at 4.91, 8.08, and 3.94 eV, respectively.

3.5.6 Energy Loss Function

The loss function $L(\omega)$ is another crucial optical parameter that helps to understand how photon energy is captured by electrons. The energy loss function quantifies the energy lost by electrons during their interaction with photons. This provides an explanation for the material's typical behavior, which is that of a conductor or plasmonic medium. Researchers are conducting research on electron energy distribution in optoelectronic devices to enhance their effectiveness [69]. There are three different ways to classify the electrons that are producing an influence on the current allocation of energy. In the beginning, the valence electrons that are positioned in the outer shell experience a process that is referred to as valence-loss. This is a process in which the valence electrons relinquish their energy as a consequence of an inter-band transition from the filled the VB to the unoccupied CB. In addition, the term "core-loss" is widely used to refer to the type of energy loss that occurs when electrons in the inner shell are excited. The third scenario is one in which the electrons either display elastic interactions or preserve their scattering to a minimum, which is frequently referred to as Zero-Loss [57, 63–66, 68]. The electrons are responsible for the energy losses that take place as a result of their absorption of photon energy. When incident photons are absorbed, the substance experiences transition due to the excitation of electrons. There are two different ways in which the transition appears. One of the occurrences comprises the transition from the VB to the CB, while the other process causes the electrons that are positioned in the valence-band to be perturbed. First, there was the electrical conductivity class of transition, and then there was the plasma frequency class, which deals with the occurrence of plasma frequency. The spectra of the loss-function typically depict the plasma frequency along with optical qualities in the region of $0 - 10$ eV. In the form of $\varepsilon(\omega)$, $L(\omega)$ may be expressed as.

$$L(\omega) = \left(\frac{-1}{\varepsilon_1(\omega)} \right) \tag{23}$$

The plasmon peak, which is the maximum figure on the $L(\omega)$ profile, is a behavior that occurs as a result of the excitation of plasmons inside the substance [68]. A representation of the $L(\omega)$ curve for $TaCu_3X_4(X = S, Se, Te)$ compounds is shown in Fig. 6g. The compounds $TaCu_3S_4$, $TaCu_3Se_4$ and $TaCu_3Te_4$ have the maximum peaks of $L(\omega)$ at 4.88, 6.46, 6.21 eV are 0.47, 0.71, and 0.63, respectively.

When $TaCu_3Se_4$ is compared to its equivalent compound under investigation, it is evident that there are higher energy losses.

3.5.7 Optical Conductivity

In the event that incident photons collide with the surface of a substance, photo-electrons are ejected from the surface of the substance. This phenomenon is known as photoelectric effect. And which is responsible for this mechanism, is defined by the optical conductivity $\sigma(\omega)$. The optical conductivity of a substance plays a crucial role in describing its behavior in the presence of an electromagnetic field. When exposed to light, the substance's optical conductivity represents its ability to transmit an electric current. It is helpful in evaluating the components of photovoltaic cells alon with photodetectors [69]. In addition to this, it is significant in determining bond-breaking when incoming radiation interacts with the surface of the substance. In Fig. 6h, the spectrum of $\sigma(\omega)$ for $TaCu_3X_4(X = S, Se, Te)$ compounds are presented. These spectra represent the conductivity of electrons in the compounds that were studied when they are subjected to electromagnetic waves. According to the data shown in Fig. 6h, it is evident that the $TaCu_3Te_4$ exhibits a higher value of optical conductivity in comparison to the $TaCu_3S_4$ and $TaCu_3Se_4$ compounds.

3.6 Thermoelectric Properties

Thermoelectric (TE) materials have attracted a lot of interest as an alternative for conventional sources of electrical energy. A variety of thermoelectric attributes make it possible to ascertain whether or not a material is suitable for use in thermoelectric appliances. The $TaCu_3X_4(X = S, Se, Te)$ materials are frequently employed in the manufacturing of electronic appliances. So, it is important to understand how they behave differently in thermoelectric parameters [70]. A thermoelectric appliance should have low thermal conductivity as well as low electrical resistivity for optimal performance [71, 72]. The functionality of thermoelectric appliances requires the study of thermoelectric properties. The Boltzmann equation is frequently applied in DFT to investigate these attributes [73]. The classical transport theory provides the foundation for the BoltzTraP algorithm. The chemical potential $[\mu(R_y)]$ is used to investigate the most important thermoelectric parameters, such as Seebeck coefficient (S), electrical conductivity (σ/τ), thermal conductivity (κ/τ) and Power-Factor [8] at the temperature range of 300–450 K and are shown by Fig. 6 in vertically aligned panels (i), [74] and [74] for $TaCu_3S_4$, $TaCu_3Se_4$ and $TaCu_3Te_4$ compounds respectively.

In thermoelectric materials, the S, also known as thermopower, is a measurement of the material's capacity to

generate an electric current in responds to temperature difference. A thermoelectric efficiency of substance may be evaluated with the help of the S. The potential gradient that is produced as a consequence of the temperature differential is used to compute the S [75, 76]. The findings of S are $-$ve when the carriers are electrons and $+$ve when the carriers are holes. Moreover, $\mu(R_y)$ with negative findings indicates p-type and positive findings of $\mu(R_y)$ indicates n-type behavior of a substance [51]. The computed maximum value of S for $TaCu_3S_4$ is $1.58(mV/K)$ at 400K, then continually goes to negative figure of $-1.58(mV/K)$ at 450K. Additionally, for $TaCu_3Se_4$ S acquire a positive figure of $1.58(mV/K)$ at 450K, then continually goes to negative figure of $-1.58(mV/K)$ at 400 and 450K. Furthermore, for $TaCu_3Te_4$ the value of S achieves a maximum finding of $1.58(mV/K)$ at 350K, then continually goes to negative figure of $-1.58(mV/K)$ at 350K with chemical potential as shown in Fig. 6a–c, respectively. The subsequent relation connects the two components of the factor κ, which are the electronic component κ_e along with the lattice component κ_{ph} [77].

$$\kappa = \kappa_{ph} + \kappa_e \tag{24}$$

Only κ_e has been included in the present study because of the constraints imposed by the BoltzTraP simulation. It has been obvious from the previous study that band gaps along with electrical behavior have a substantial impact on the thermoelectric characteristics of a material [78]. The materials that have small band gaps are excellent prospects for applications in the thermoelectric power industry. Figure 6 illustrates how electrons in narrow band gap semiconductors possess the ability to migrate readily from the valence band to the conduction band, which results in an increase in electric conductivity and a decrease in thermal conductivity. Figure 6 also depicts that the calculated findings illustrate the presence of the n-type along with p-type charge carriers for positive as well as negative figures of $\mu(R_y)$. The electrical conductivity in substances is affected by the passage of carriers through them, which is important for thermoelectric functions. Both the $+$ve as well as $-$ve figures of $\mu(R_y)$ are associated with the allocation of electrons as well as holes to conduction, as seen in Fig. 6d–f for $TaCu_3S_4$, $TaCu_3Se_4$, and $TaCu_3Te_4$ compounds, respectively. Figure 6d–f illustrates the respective contributions of electrons along with holes to the process of conduction. These contributions are correlated with both negative and positive values of $\mu(R_y)$. According to the findings, highest peak figure of electrical conductivity for $TaCu_3S_4$, $TaCu_3Se_4$, and $TaCu_3Te_4$ compounds are 19.84×10^{19}, 23.18×10^{19}, and $19.84 \times 10^{19} (\Omega ms)^{-1}$, occurring at 300K, respectively. The present findings also display that the majority of carriers are electrons.

The movement of carriers through compounds has an impact on the thermal conductivity of such compound, which is an essential factor for the function of thermoelectric appliances. Specifically, the contributions of electrons as well as holes to the phenomenon of conduction are shown in Fig. 6g–i corresponding to configuration. It has been shown that these contributions reflect a correlation with a variety of negative along with positive values of $\mu(R_y)$. Based on the observations, it has been illustrate that the maximum peak figure of electrical conductivity for $TaCu_3S_4$, $TaCu_3Se_4$, and $TaCu_3Te_4$ compounds is 19.39×10^{14}, 21.67×10^{14}, and $20.57 \times 10^{14} W(m.K.s)^{-1}$ occurring at 0.84, 0.82, and 0.80 eV, accordingly. These findings show maximum values at 450 K temperature. As a result of the data presented here, it has been established that the vast majority of carriers are electrons.

In order to determine the output efficiency of a compound, the power factor [8] is an essential component to consider. The PF and S have a direct relationship to each, higher the figures of PF are characterized by the large findings of the S [79]. Moreover, following relation is implemented to get the PF [14].

$$PF = \sigma S^2 \tag{25}$$

Figure 6j–l depicts the computed value of the understudies compounds. For $TaCu_3S_4$, compound, power factor attains a maximum value of 0.44 T at 400 K. For $TaCu_3Se_4$, and $TaCu_3Te_4$, the PF represents an increasing profile as the temperature is increased plus gains a maximum value of 0.47 and 0.51 T occurring at 300 K and 450K, respectively. Based on the results obtained in current computation, it is evident that our understudied compounds are the best fit for thermoelectric applications.

The need for materials containing Ta-Series compounds stems from their potential to enhance energy and environmental performance. These components have high Seebeck coefficients along with low lattice thermal conductivity, which means that they are efficient in thermoelectricity generators and refrigeration devices. We want to use sulfide materials in optoelectronics, like photovoltaic materials and photocatalysts, because they have large optical values and indirect band gaps of 1.71 eV for S, 1.65 eV for Se, and 0.14 eV. The structural robustness, chemical composition ratios, and mechanical properties enhance the use of these materials in a variety of technologies. Moreover, the use of non-toxic elements throughout the earth increases sustainability and environmental friendliness. Therefore, we can conclude that members of the Ta-series compounds contribute to the development of sustainable technology by providing energy that both meets societal demands and aligns with environmental requirements (Fig. 7).
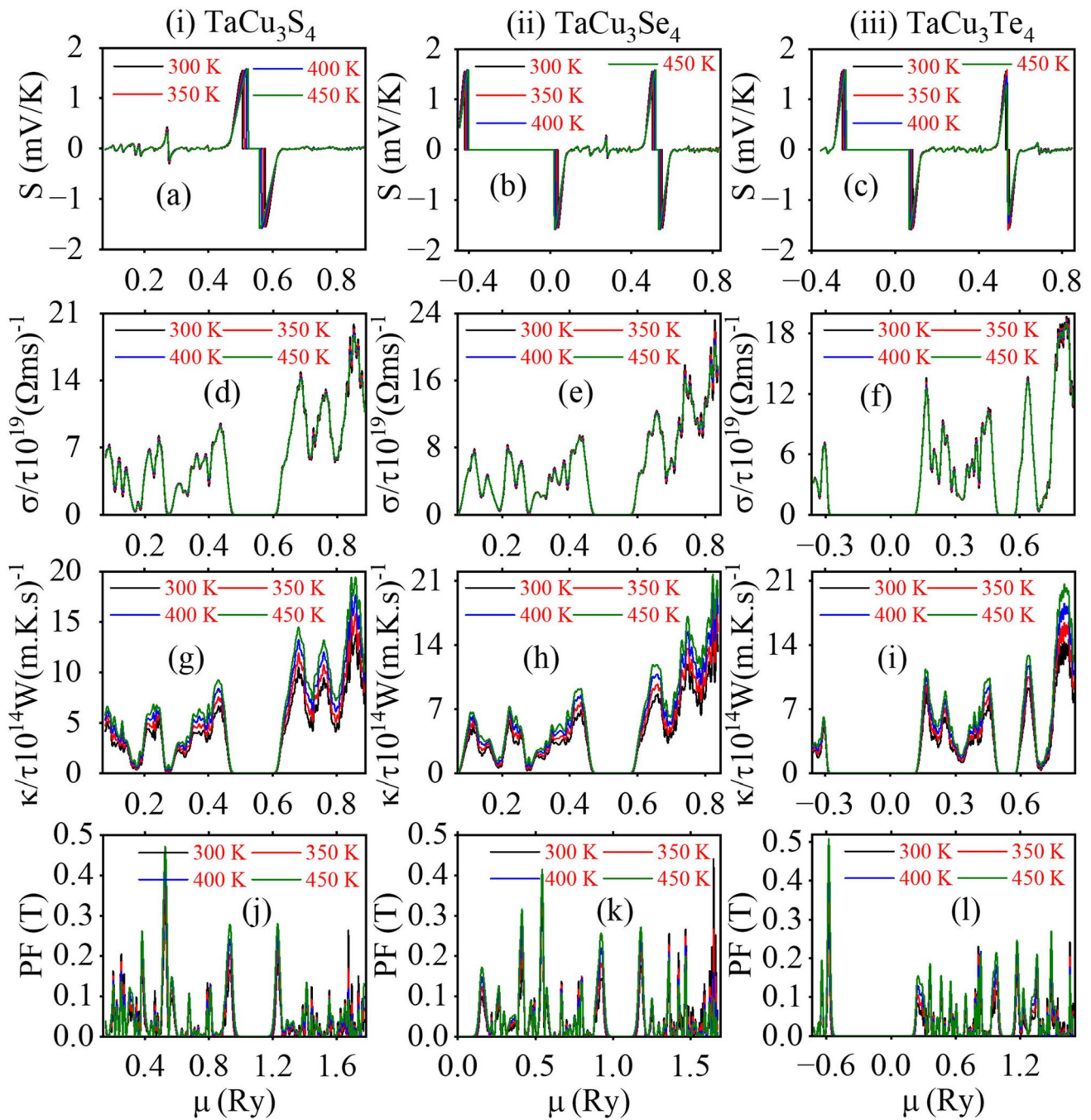
Fig. 7 The investigated thermoelectric properties for the TaCu$_3$X$_4$(X = S, Se, Te) compounds

4 Conclusion

The study utilizes the First-Principle computational technique to explore the structural, mechanical, electronic, thermodynamic, optical, as well as thermoelectric attributes of the TaCu$_3$X$_4$(X = S, Se, Te) chemicals. The study aimed to identify the most stable profile of TaCu$_3$X$_4$ chemicals. The structural stability of underlying compounds was evaluated through the computation of binding energy along with lattice constants. The research indicates that the chemicals TaCu$_3$S$_4$, TaCu$_3$Se$_4$, and TaCu$_3$Te$_4$ exhibit structural stability, with lattice parameters of 5.55, 5.45, and 6.01 Å respectively. The elastic stiffness constant assessment is utilized to evaluate the mechanical stability of the materials. The selected compounds have been theoretically confirmed to possess a significant degree of mechanical stability. The brittleness of the studied compounds can

be determined through the analysis of Passion and Pugh's ratios plus the Cauchy pressure. The study evaluated the electronic attributes of $TaCu_3S_4$, $TaCu_3Se_4$, and $TaCu_3Te_4$ chemicals, revealing indirect band gaps of 0.71, 1.60, and 1.15 eV, respectively. In order to understand the unique contributions of different states to the diverse band structure, computations for both TDOS plus PDOS are ascertained. The study computes thermodynamic characteristics at zero (0 GPa) pressure, including vibrational energy, free energy, Debye entropy, as well as heat capacity against temperature, revealing a declining vibration free energy pattern. Various optical parameters, including absorption-coefficient, optical-reflectivity, dielectric-function components, optical conductivity, as well as electron energy loss-function, have been determined through calculations. The studied materials exhibit exceptional optical conductivity plus absorption coefficients when exposed to an energetic photon beam, but exhibit opacity at low energies. The selected compounds may eventually transform into TE materials that can function even at high temperatures, based on their estimated TE characteristics. The current study may offer guidance for future researchers aiming to develop innovative optoelectronic and TE technologies with exceptional stability.

Author Contributions The Author, S.U.A. and M.E.M., suggest the idea. M.T., M.B., and D.k. calculated the properties of material. M.A.I., A.M.S., G.F.B.S., A.A.E., M.M.A., and all authors analyzed the data. All the authors helped to write the initial draft and helped to improve the manuscript till the final version. The manuscript was written with contributions from all authors. All authors have approved the final version of the manuscript.

Data Availability No datasets were generated or analysed during the current study.

Declarations

Competing Interest The authors declare no competing interests.

References

1. X. Zhang et al., A novel aluminum–graphite dual-ion battery. Adv. Energy Mater. **6**(11), 1502588 (2016)
2. M. Wang et al., Reversible calcium alloying enables a practical room-temperature rechargeable calcium-ion battery with a high discharge voltage. Nat. Chem. **10**(6), 667–672 (2018)
3. C. Zhu et al., An innovative process design and multi-criteria study/optimization of a biomass digestion-supercritical carbon dioxide scenario toward boosting a geothermal-driven cogeneration system for power and heat. Energy **292**, 130408 (2024)
4. A. Hong et al., Novel p-type thermoelectric materials Cu 3 MCh 4 (M = V, Nb, Ta; Ch = Se, Te): high band-degeneracy. Journal of Materials Chemistry A **5**(20), 9785–9792 (2017)
5. R. Martins, Materials as activator of future global science and technology challenges. Prog. Nat. Sci.: Mater. Int. **31**(6), 785–791 (2021)
6. M.K. Bilal et al., Enhanced energy storage properties of 0.7 Bi0·5Na0 5TiO$_3$–0.3 SrTiO$_3$ ceramic through the addition of NaNbO3. Ceram. Int. **47**(21), 30922–30928 (2021)
7. T.M. Tritt, M. Subramanian, Thermoelectric materials, phenomena, and applications: a bird's eye view. MRS Bull. **31**(3), 188–198 (2006)
8. P. Newhouse et al., Thin film preparation and characterization of wide band gap Cu3TaQ4 (Q = S or Se) p-type semiconductors. Thin Solid Films **517**(7), 2473–2476 (2009)
9. X.-P. Liu et al., Promising thermoelectric materials of Cu3VX4 (X= S, Se, Te): A Cu-VX framework plus void tunnels. Int. J. Mod. Phys. C **30**(08), 1950045 (2019)
10. K. Suekuni et al., High-performance thermoelectric minerals: colusites Cu26V2M6S32 (M= Ge, Sn). Appl. Phys. Lett. (2014). https://doi.org/10.1063/1.4896998
11. P. Grima-Gallardo et al., Cu3TaSe4 and Cu3NbSe4: X-ray diffraction, differential thermal analysis, optical absorption and Raman scattering. J. Alloy. Compd. **658**, 749–756 (2016)
12. Y. Ju et al., Distributed three-phase power flow for AC/DC hybrid networked microgrids considering converter limiting constraints. IEEE Trans. Smart Grid **13**(3), 1691–1708 (2022)
13. M. Abubakr et al., Systematic study on the optoelectronic and elastic properties of Cu-based ternary chalcogenides: using ab-initio approach. Mater. Sci. Semicond. Process. **162**, 107512 (2023)
14. !!! INVALID CITATION !!! .
15. Z. Abbas et al., Density-functional quantum analysis of optoelectronic, elastic, thermodynamic and hydrogen storage properties of AMgH3 (A= be, ca) perovskite-type hydrides: Prospects for clean energy hydrogen-storage fuel and optoelectronic applications. Int. J. Hydrogen Energy **60**, 212–228 (2024)
16. P. Giannozzi et al., QUANTUM ESPRESSO: a modular and open-source software project for quantum simulations of materials. J. Phys. Condens. Matter **21**(39), 395502 (2009)
17. P. Giannozzi et al., Quantum ESPRESSO toward the exascale. J. Chem. Phys. (2020). https://doi.org/10.1063/5.0005082
18. A. Gencer, G. Surucu, Properties of BaYO3 perovskite and hydrogen storage properties of BaYO3Hx. Int. J. Hydrogen Energy **45**(17), 10507–10515 (2020)
19. S. Al, M. Yortanlı, E. Mete, Lithium metal hydrides (Li2CaH4 and Li2SrH4) for hydrogen storage; mechanical, electronic and optical properties. Int. J. Hydrogen Energy **45**(38), 18782–18788 (2020)
20. N. Troullier, J.L. Martins, Efficient pseudopotentials for plane-wave calculations. Phys. Rev. B **43**(3), 1993 (1991)
21. Blaha, P., et al., WIEN2k, An Augmented Plane Wave Plus Local Orbitals Program for Calculating Crystal Properties (Vienna University of Technology, Austria, 2001). Google Scholar There is no corresponding record for this reference. 2002.
22. V. Jafari-Sadeghi et al., Understanding the De-internationalization of entrepreneurial SMEs in a volatile context: a reconnoitre on the unique compositions of internal and external factors. Br. J. Manag. **34**(4), 2116–2137 (2023)
23. N. Marzari et al., Thermal contraction and disordering of the Al (110) surface. Phys. Rev. Lett. **82**(16), 3296 (1999)
24. G. Kerker, Non-singular atomic pseudopotentials for solid state applications. J. Phys. C Solid State Phys. **13**(9), L189 (1980)
25. B.G. Pfrommer et al., Relaxation of crystals with the quasi-Newton method. J. Comput. Phys. **131**(1), 233–240 (1997)

26. J.P. Perdew, K. Burke, M. Ernzerhof, Generalized gradient approximation made simple. Phys. Rev. Lett. **77**(18), 3865 (1996)
27. P. Borlido et al., Validation of pseudopotential calculations for the electronic band gap of solids. J. Chem. Theory Comput. **16**(6), 3620–3627 (2020)
28. M. Rkhis et al., First principle investigation on hydrogen solid storage in Zr1-xNbxNiH3 (x= 0 and 0.1). Int. J. Hydrogen Energy **44**(41), 23188–23195 (2019)
29. Haque, E., Effect of electron-phonon scattering, pressure and alloying on the thermoelectric performance of TmCu $ _3 $ Ch $ _4 $(Tm= V, Nb, Ta; Ch= S, Se, Te). arXiv Preprint arXiv:2010.08461, 2020.
30. M. Ali et al., Structural, optoelectronic and thermodynamical insights into 2H-ZrO2: A DFT investigation. Inorg. Chem. Commun. **160**, 111891 (2024)
31. B. Zhai et al., First-principles prediction of potential candidate materials M Cu 3 X 4 (M= V, Nb, Ta; X= S, Se, Te) for neuromorphic computing. Phys. Rev. Appl. **19**(5), 054045 (2023)
32. W. Belkilali et al., Theoretical investigations of structural, mechanical, electronic and optical properties of NaScSi alloy. Emergent Materials **4**, 1465–1477 (2021)
33. Lamichhane, A., First-principles density functional theory studies on perovskite materials. 2021, New Jersey Institute of Technology.
34. X. Liu, J. Fu, First principle study on electronic structure, elastic properties and debye temperature of pure and doped KCaF3. Vacuum **179**, 109504 (2020)
35. M. Born, On the stability of crystal lattices I, in *Mathematical proceedings of the cambridge philosophical society*. (Cambridge University Press, 1940)
36. F. Mouhat, F.-X. Coudert, Necessary and sufficient elastic stability conditions in various crystal systems. Phys. Rev. B **90**(22), 224104 (2014)
37. C. Campos et al., Influence of minor oxidation of the precursor powders to form nanocrystalline CdTe by mechanical alloying. J. Alloy. Compd. **466**(1–2), 80–86 (2008)
38. B. Rehmat et al., Elastic properties of perovskite-type hydrides LiBeH3 and NaBeH3 for hydrogen storage. Int. J. Hydrogen Energy **42**(15), 10038–10046 (2017)
39. A. Reuß, Berechnung der fließgrenze von mischkristallen auf grund der plastizitätsbedingung für einkristalle. ZAMM-J. Appl. Math. Mechanics/Zeitschrift für Angewandte Mathematik und Mechanik **9**(1), 49–58 (1929)
40. Voigt, W. and W. Voigt, Wechselbeziehungen zwischen zwei Tensortripeln.(Elastizität und innere Reibung.). 1966: Springer
41. R. Hill, The elastic behaviour of a crystalline aggregate. Proc. Phys. Soc. Sect. A **65**(5), 349–354 (1952)
42. X. Liu et al., First-principles study on electronic structure elasticity debye temperature and anisotropy of cubic KCaF3, in *Materials science forum*. (Trans Tech Publ, 2020)
43. M. Garara et al., Hydrogen storage properties of perovskite-type MgCoH$_3$ under strain effect. Mater. Chem. Phys. **254**, 123417 (2020)
44. K.M. Hossain, M.Z. Hasan, M.L. Ali, Understanding the influences of Mg doping on the physical properties of SrMoO3 perovskite. Results Phys. **19**, 103337 (2020)
45. Z.-J. Wu et al., Crystal structures and elastic properties of superhard Ir N 2 and Ir N 3 from first principles. Phys. Rev. B **76**(5), 054115 (2007)
46. M.H. Murad, S. Fatema, Some static relativistic compact charged fluid spheres in general relativity. Astrophys. Space Sci. **350**, 293–305 (2014)
47. D. Iotova et al., Chemical bonding and elastic constants of nickel-based intermetallics, in *Properties of complex inorganic solids*. (Springer, Bostan, 1997), pp.389–395
48. S. Qiu et al., Local-ordering mediated configuration stability and elastic properties of aluminum-containing high entropy alloys. Intermetallics **110**, 106474 (2019)
49. S.L. Wang, Y. Pan, Insight into the structures, melting points, and mechanical properties of NbSi2 from first-principles calculations. J. Am. Ceram. Soc. **102**(8), 4822–4834 (2019)
50. Schreiber, E., et al., Elastic constants and their measurement. 1975.
51. R.E. Hummel, R.E. Hummel, Electrical properties of polymers, ceramics, dielectrics, and amorphous materials, in *Electronic properties of materials*. (Springer, NY, 2011), pp.181–211
52. P. Dufek, P. Blaha, K. Schwarz, Applications of Engel and Vosko's generalized gradient approximation in solids. Phys. Rev. B **50**(11), 7279 (1994)
53. Z. Charifi et al., High pressure study of structural and electronic properties of calcium chalcogenides. J. Phys. Condens. Matter **17**(26), 4083 (2005)
54. Z. Abbas et al., First-principles calculations to investigate electronic, optical, and thermoelectric properties of Na2GeX3 (X= S, Se, Te) for energy applications. Mater. Sci. Semicond. Process. **154**, 107206 (2023)
55. M. Abubakr et al., Study of structural, optoelectronic and magnetic properties of Half-Heusler compounds QEuPa (Q= Ba, be, Mg, Sr) using first-principles method. J. Solid State Chem. **304**, 122612 (2021)
56. S. Sahoo et al., Silicene: an excellent material for flexible electronics. J. Phys. D Appl. Phys. **55**(42), 425301 (2022)
57. N. Rahman et al., First-principles calculations to investigate structural, elastic, optical, and thermoelectric properties of narrow band gap semiconducting cubic ternary fluoroperovskites barium based BaMF3 (M= Ag and Cu) compounds. J. Market. Res. **21**, 2168–2177 (2022)
58. S.H.A. Jaffery et al., Strong interlayer transition in a staggered gap GeSe/MoTe2 heterojunction diode for highly efficient visible and near-infrared photodetection and logic inverter. EcoMat **5**(3), e12307 (2023)
59. S.H.A. Jaffery et al., Near-direct band alignment of MoTe2/ReSe2 Type-II p-n heterojunction for efficient VNIR photodetection. Adv. Mater. Technol. **7**(10), 2200026 (2022)
60. J.R. Thompson et al., Spatial simulation of codesigned land cover change scenarios in New England: alternative futures and their consequences for conservation priorities. Earth's Future (2020). https://doi.org/10.1029/2019EF001348
61. F. Colmenero et al., Thermodynamic properties of uranyl-containing materials based on density functional theory. J. Phys. Chem. C **122**(10), 5254–5267 (2018)
62. H.-X. Gao et al., First-principles study on the structural, electronic, elastic, optical and thermodynamic properties of double antiperovskites X6BiSbN2 (X= Mg, Ca, Sr). J. Phys. Chem. Solids **187**, 111859 (2024)
63. M. Ali et al., Layer-sliding-mediated controllable synthetic strategy for the preparation of multifunctional materials. Mater. Today Commun. **37**, 107022 (2023)
64. M. Younis et al., Layer-sliding-mediated reversible tuning of interfacial electronic and optical properties of intercalated ZrO2/MoS2 van der Waals heterostructure. J. Mater. Res. **38**(23), 4995–5007 (2023)
65. M. Ali, M. Yousaf, J. Munir, Achieving controllable multifunctionality through layer sliding. J. Mol. Graph. Model. **126**, 108638 (2024)
66. M. Ali et al., CO Adsorption on two-dimensional 2H-ZrO2 and its effect on the interfacial electronic properties: implications for sensing. Phys. Scr. **98**(11), 115801 (2023)
67. S.H. Mirza et al., Enlightening the impact of TM doping on structural, electronic and magnetic properties of ceria for ReRAM

applications: a GGA+ U study. Chem. Pap. **77**(9), 5481–5494 (2023)

68. F. Laquai, A. Mishra, M. Ribas, et al., Photophysical properties of a series of poly(ladder-type phenylene)s†. Adv. Funct. Mater. **17**, 3231 (2007)

69. Z. Abbas et al., First-principles calculations to investigate structural, electronic, optical and magnetic properties of pyrochlore oxides Eu2Tm2O7 (Tm= Hf, Sn, Zr) for energy applications. Inorganics **11**(5), 193 (2023)

70. V. Srivastava et al., Investigation of the electronic, magnetic, elastic, thermodynamic and thermoelectric properties of Mn2CoCr Heusler compound: A DFT-based simulation. J. Magn. Magn. Mater. **513**, 167107 (2020)

71. J. He et al., Ultralow thermal conductivity in full Heusler semiconductors. Phys. Rev. Lett. **117**(4), 046602 (2016)

72. H. Nakatsugawa et al., Thermoelectric properties of heusler Fe 2 TiSn Alloys. J. Electron. Mater. **49**, 2802–2812 (2020)

73. A. Minnich et al., Bulk nanostructured thermoelectric materials: current research and future prospects. Energy Environ. Sci. **2**(5), 466–479 (2009)

74. M.L. Tushman, C.A. O'Reilly III., Ambidextrous organizations: managing evolutionary and revolutionary change. Calif. Manage. Rev. **38**(4), 8–29 (1996)

75. A. Yamada, S.-C. Chung, K. Hinokuma, Optimized LiFePO4 for lithium battery cathodes. J. Electrochem. Soc. **148**(3), A224 (2001)

76. G. Nolas, D. Morelli, T.M. Tritt, Skutterudites: a phonon-glass-electron crystal approach to advanced thermoelectric energy conversion applications. Annu. Rev. Mater. Sci. **29**(1), 89–116 (1999)

77. Y. Chen, J. Ma, W. Li, Understanding the thermal conductivity and Lorenz number in tungsten from first principles. Phys. Rev. B **99**(2), 020305 (2019)

78. G. Nazir et al., Study of narrow band gap double perovskites (Sr/Ba) 2BB'O6 (B= In, Tl, B'= Sb, Bi) for optical, thermoelectric, and mechanical properties. Mater. Today Commun. **31**, 103547 (2022)

79. Banik, A., M. Agne, and W. Zeier, *5.3* Materials for thermoelectric devices. Applied Inorganic Chemistry. **26**